Journal of Geophysical Research: Solid Earth

RESEARCH ARTICLE
10.1029/2018JB016270

Induced Earthquake Families Reveal Distinctive Evolutionary Patterns Near Disposal Wells

Elizabeth S. Cochran[1], Zachary E. Ross[2], Rebecca M. Harrington[3], Sara L. Dougherty[1], and Justin L. Rubinstein[4]

[1]U.S. Geological Survey, Pasadena, CA, USA, [2]California Institute of Technology, Pasadena, CA, USA, [3]Ruhr-Universität Bochum, Bochum, Germany, [4]U.S. Geological Survey, Menlo Park, CA, USA

Key Points:
- Near-repeated earthquake families close to disposal wells show different interevent time evolution than those at greater distances
- Families near wells show near-Poissonian interevent times, while families at greater distances are more highly clustered
- Increasing pore-fluid pressures likely controls the timing of earthquake sequences close to wells

Supporting Information:
- Supporting Information S1
- Data Set S1

Correspondence to:
E. S. Cochran,
ecochran@usgs.gov

Citation:
Cochran, E. S., Ross, Z. E., Harrington, R. M., Dougherty, S. L., & Rubinstein, J. L. (2018). Induced earthquake families reveal distinctive evolutionary patterns near disposal wells. *Journal of Geophysical Research: Solid Earth*, *123*, 8045–8055. https://doi.org/10.1029/2018JB016270

Received 22 JUN 2018
Accepted 10 SEP 2018
Accepted article online 14 SEP 2018
Published online 28 SEP 2018

Abstract The timing of events in seismic sequences can provide insights into the physical processes controlling fault slip. In southern Kansas, the rate of earthquakes rose rapidly starting in 2013 following expansion of energy production into the area, demanding the disposal of large volumes of wastewater into deep wells. Seismicity catalogs that are complete to low magnitudes can provide insights into the physical processes that induce seismicity near wastewater disposal. We develop a catalog of over 130,000 earthquakes recorded in southern Kansas from mid-March 2014 through December 2017 by applying a matched filter algorithm to an original catalog of 5,831 template earthquakes. Detections have nearly identical waveforms to their associated template event and represent slip on nearly co-located sections of a fault. We select template events with at least 100 associated detections and examine the characteristics of these prolific families of earthquakes. We find that families located close (<10 km) to areas with significant volumes of injected fluids have near-Poissonian interevent times and the families remain active over longer durations. Families farther from high-volume injection wells show strong clustering of interevent times and shorter sequence durations. We conclude that increasing pore fluid pressures from nearby disposal of large volumes of wastewater is the primary driver of these long duration episodes, with earthquake-earthquake interactions driving sequences at greater distance from the wells.

1. Introduction

Seismicity rates in the central United States have soared in recent years following expansion of energy production that required the disposal of unprecedented volumes of fluid byproducts (wastewater) into deep wells (Ellsworth, 2013). Oklahoma and Kansas saw the largest increases in earthquake rates with peak annual seismicity rates rising significantly compared to background rates. There, the primary target of wastewater disposal is the Arbuckle Group, an underpressured, highly permeable formation that lies in direct contact with the highly fractured Precambrian basement rocks below (e.g., Franseen et al., 2004; Morgan & Murray, 2015). A subset of basement faults extend up into overlying sediments, cutting through the Arbuckle Group and providing direct pore-fluid pressure pathways for injected fluids to reach the basement faults (Schwab et al., 2017). Earthquake triggering by fluid migration has been observed in both natural and induced sequences (e.g., Parotidis et al., 2005; Ross, Rollins, et al., 2017; Shelly et al., 2016), where erosion in fault strength occurs as pore fluid pressures rise and reduce the effective normal stress (Byerlee, 1993; Sibson, 1992). Spatiotemporal correlations between seismicity and high-volume wastewater injection (Healy et al., 1968; Keranen et al., 2013; Walsh & Zoback, 2015) suggest that pore fluid pressure increases resulting from injection can cause slip on basement faults (Kroll et al., 2017; Nicholson & Wesson, 1990; Rayleigh et al., 1976; Talwani et al., 2007; Wang, 2000; Zoback, 2007).

Injection-induced pressure changes have been shown to result in both seismic and aseismic slips. For example, Wei et al. (2015) observed that the 2012 Brawley, California swarm was preceded by aseismic slip beneath a nearby geothermal field. Cornet et al. (1997) showed that microseismicity recorded near an injection site accounted for only a small fraction of the total observed slip and concluded much of the slip was aseismic. Similar observations were made at an in situ subsurface laboratory, where aseismic slip was shown to occur within the fluid pressurized zone and aseismic creep mediated the occurrence of microearthquakes (Guglielmi et al., 2015). However, aseismic slip can be difficult to detect without direct access to measure accumulated slip on basement faults, so studies in the central United States have predominantly focused on analysis of seismic events. Induced earthquake sequences exhibit a wide range of temporal behavior;

some sequences display little to no temporal clustering, while others exhibit strong temporal clustering (e.g., Schoenball & Ellsworth, 2017a), such as mainshock-aftershock sequences (e.g., Keranen et al., 2013) or swarms of similar-sized events (e.g., Horton, 2012).

The behavior of induced earthquake sequences can provide insights into the physical mechanisms driving the sequences (e.g., Schoenball & Ellsworth, 2017b) and improve estimates of the resulting hazard (Petersen et al., 2015). An easily observable and often-studied characteristic of spatially clustered seismic events (earthquakes and tremor) is the time between events, also known as the interevent time or recurrence time. The distribution of interevent times can be used to classify seismic sequences, such that sequences with Poissonian recurrence times can be separated from those that are quasi-periodic or temporally clustered (Kagan & Jackson, 1991). Interevent time distributions have been correlated to various source properties, such as rupture velocity, or material properties, such as porosity, fluid pressures, or fault strength (e.g., Blanpied et al., 1992; Nadeau & Johnson, 1998; Shelly & Johnson, 2011; Sibson, 1992).

Further, the identification of earthquakes with nearly identical waveforms, A.K.A. repeating earthquakes, suggests recurring slip along co-located, or nearly so, patches of fault (e.g., Geller & Mueller, 1980; Nadeau & McEvilly, 1999; Vidale et al., 1994). Repeating earthquakes have been used to probe spatial and temporal variations in fault strength and are often interpreted as repeated failure of an asperity embedded in an aseismically creeping fault (e.g., Bufe et al., 1977; Nadeau & Johnson, 1998). Other mechanisms can also result in recurring slip. For example, repeating earthquakes observed during the fluid injection experiment at the KTB deep drilling site in Germany (Zoback & Harjes, 1997) were interpreted as repeated failure of well-oriented fractures while fluid pressures steadily increased (Baisch & Harjes, 2003).

Here we examine seismicity in a region of southern Kansas where earthquake rates rose dramatically starting in late 2013, peaked in 2015, and have since decreased following reductions in injected volumes due to regulations and economics (Peterie et al., 2018; Rubinstein et al., 2018). A local seismic network installed in 2014 captures the rise, and subsequence decrease, in seismicity across the region and provides a unique dataset with which to examine the evolutionary patterns of seismic sequences at a range of distances from high-rate injection wells (Rubinstein et al., 2018). We expand the catalog of Rubinstein et al. (2018) using a matched filter technique to detect families of earthquakes with nearly identical waveforms. We examine the distribution of interevent times measured on a set of 130 prolific earthquake families with at least 100 events each to infer physical processes driving the sequences.

2. Data and Methods

We used 18 stations within 80 km of the study center that recorded seismic data for the period from 21 March 2014 to 31 December 2017 (Table S1 in the supporting information). The stations were from the GS and OK networks. We use as template events a catalog of 5,831 earthquakes covering the period from 21 March 2014 through 31 December 2017 that is complete to magnitude 2 after 1 July 2014 (Figure 1). The template catalog is from Rubinstein et al. (2018), updated to include events through the end of 2017 (Data File S1 in the supporting information). We use relocations of the catalog events where available, or standard locations otherwise. Raw 24-hr seismic data files were processed to remove gaps, detrended, bandpass filtered between 2 and 15 Hz using a 4-pole filter, and then decimated to 50 samples per second. Data files were rejected (not processed) if the gaps total more than 10% of the 24-hr file length.

We used the matched filter method of Ross, Hauksson, et al. (2017), based on Shelly et al. (2016), to detect additional earthquakes in the continuous data. Template waveforms were extracted as 2.0-s windows starting 0.5 s before the *P* and *S* phase picks on all three components for each template event. To ensure no overlap with the *S* wave, the windows were shortened to the *S-P* times if the *S-P* time is less than 2.0 s. Template windows were correlated against the continuous, 24-hr long processed seismic data, and cross-correlation functions are summed across all phases, channels, and stations. Detections were declared at a threshold of 9 times the median absolute deviation, if at least nine channels of data were available. For detections spaced less than 2 s apart, the template with the largest average cross correlation was selected. The location of the template event was assigned to the correlating detection(s). The magnitude was calculated from the median amplitude ratio for phases with signal-to-noise ratios of five or larger. The above procedure resulted in a detection catalog of 131,413 events.

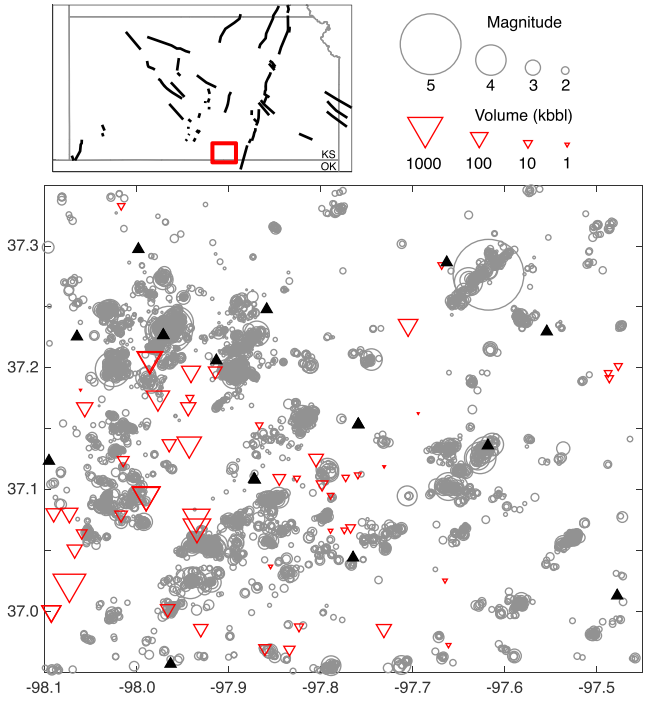

Figure 1. Map of earthquake templates. Upper left shows the location of the study area (red box) in south central Kansas. Major mapped structures are shown by bold lines (from Niemi, 2004), and state boundaries are shown by gray lines. Lower figure shows the seismic network (solid black triangles). Earthquakes (gray circles) used as template events scaled by magnitude from Rubinstein et al. (2018). The 12 November 2014 *M*4.9 Milan earthquake is the largest event shown in the northeast portion of the study area. Arbuckle wells (inverted red triangles) are shown and scaled by cumulative disposal volumes from 2012 to 2017.

3. Results

3.1. Matched Filter Detections and Identification of Prolific Families

We investigate the characteristics of seismicity in a region of high volume wastewater disposal in southern Kansas using a matched filter technique to identify near-repeating earthquakes. Matched filter methods reduce the minimum magnitude, and magnitude of completeness, for sequences of events with near-identical waveforms; however, the method is unable to detect events in regions without template events. The matched filter method produces a catalog of 131,413 detections. The full catalog has a minimum magnitude of approximately −1, a magnitude of completeness of 0.75, and a *b*-value indistinguishable from 1.0 (Figure S1 in the supporting information). The original template catalog also has a *b*-value of approximately 1 (Rubinstein et al., 2018).

Following the nomenclature of Shelly and Johnson (2011), we refer to a template with one or more associated detections as a "family." We choose not to use the term repeated events as it may suggest the same amount of slip is occurring on the same size fault patch; here the magnitudes of the template and associated detections can range from −1 to 3 within a single family. Figure 2a shows the waveforms for one family with 387 detections recorded on the horizontal component of a local station. The waveforms are aligned on the *P* phase arrival, and only minor differences (<0.1 s) in the *S* phase arrival times are apparent, suggesting that the events are located nearly equidistant from the station. Furthermore, the *S* phase waveforms, filtered between 2 and 15 Hz, are nearly identical in both duration and frequency content within the family. The variability in the rate of matched filter detections through time is similar to the temporal variability in the rate of events in the template catalog (Figure S2). Over the approximately 3.5-year study period the number of detections per template ranges from 0 to 510 detections. Figure 2b shows a histogram of the binned number of times an individual template is associated with a certain number of detections. The vast majority of templates have several tens or fewer associated detections.

In order to have a sufficient number of events to examine the time evolution of individual families we focus on families with 100 or more events. However, the results do not change significantly if we examine families with a slightly greater or fewer number of events. A total of 130 prolific families of at least 100 events each are identified from the 5,831 templates and their associated detections (Figure 2b). Figure 2c shows a map of the number of detections per template, with the prolific families highlighted. We find that prolific families are clustered in the west-northwest of the study area in a 10 km by 10 km region, in and adjacent to a region of high volume wastewater disposal. While significant volumes of wastewater (as much as ~50 million barrels in a single 0.05° × 0.05° bin) have been disposed in much of the western third of the study area, there is a dearth of seismicity, and prolific families in particular, observed in the southwest portion of the study area close to high volume wells. There are scattered prolific families across much of the rest of the region, including several families near the 12 November 2014 *M*4.9 Milan earthquake in the northeast portion of the study area.

3.2. Cumulative Event Curves and Coefficient of Variation of Interevent Times

In Figure 3 we plot the event magnitudes versus time, cumulative event curves, and histograms of the interevent time distributions for three prolific families. Differences in the temporal distribution of events between the three families are apparent. The first family (Family 1—Template 70049378) is located adjacent to a region of high volume wastewater injection and events occur fairly regularly throughout the study period, with essentially no temporal clustering of events (Figure 3a). A nearby family (Family 2—Template 70060673) displays some moderate clustering of events over periods of several months with intermittent periods of quiescence (Figure 3b). The third family (Family 3—Template 70175408) is located near the

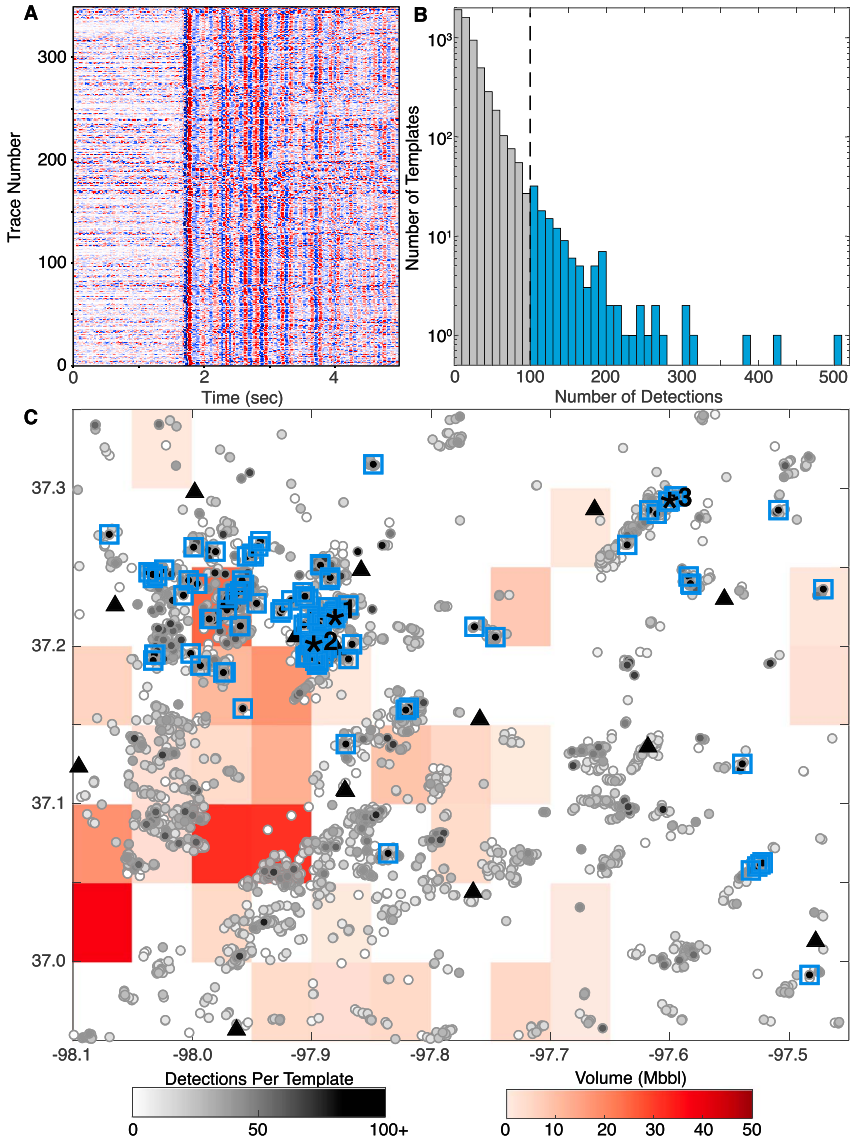

Figure 2. Detections and prolific families. (a) Detections associated with template 70124853 recorded at station KAN05 on horizontal component HHN. Waveforms are aligned with the *P* wave arrival at 0.5 s; here the visible phases are associated with the *S* wave arrival. (b) Histogram of the binned number of times an individual template is associated with a certain number of detections. A majority of the templates have fewer than 50 detections. We identify prolific families as templates with 100 or more detections (blue). (c) Map showing locations of the 130 prolific families (blue squares). The number of detections per template, plotted at the template location, is shown by the grayscale dots. The cumulative volume of wastewater disposed into the Arbuckle from 2012 to 2017 computed in 0.05° × 0.05° bins is shown by the red surface. The triangles show seismic station locations. The asterisks indicate the three prolific families that are shown in Figure 3.

*M*4.9 Milan earthquake, far from the peak injection, and shows strong clustering with a majority of events occurring over just a few days (Figure 3c). Family 3 also shows more short interevent times than Family 1, even though their mean interevent times are similar (Figure 3).

We quantify the time evolution of each prolific family by computing the coefficient of variation (Cv) of the interevent times (*T*; Kagan & Jackson, 1991). Cv is defined as the ratio of the standard deviation of the interevent times (σT) to the average interevent time ($\overline{\mathbf{T}}$) of the family. Cv quantifies the temporal behavior of earthquake occurrence and was defined to determine, for example, if (declustered) mainshocks are Poisson-distributed as has been widely suggested (e.g., Gardner & Knopoff, 1974). For a random Poissonian distribution of occurrence times Cv = 1, while Cv $<$ 1 identifies sequences that are quasi-periodic and

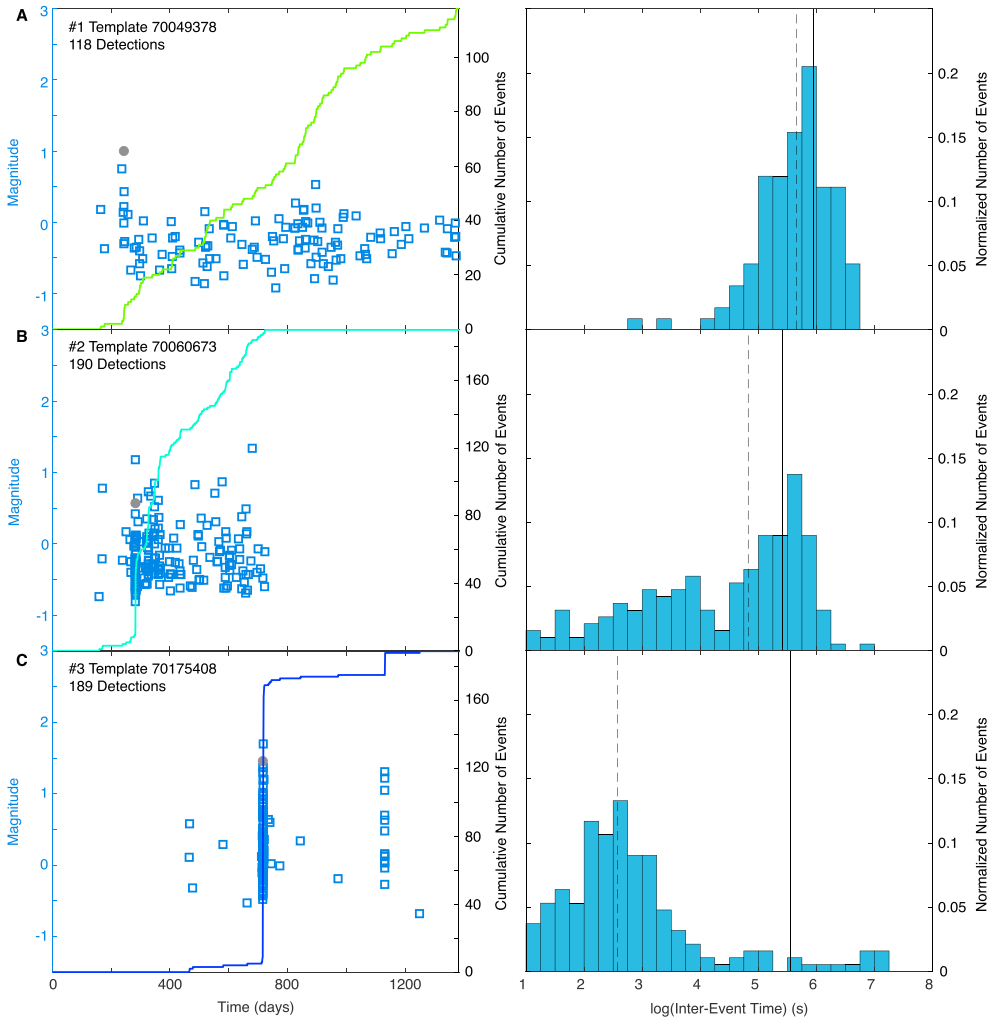

Figure 3. Sequences of prolific families. (left) Cumulative event curves (colored lines) and event magnitudes (template = gray circles; detection = blue squares) versus number of days since 03/21/2014 and (right) interevent time histograms and mean and median interevent time (black solid and dashed vertical lines) for (a) Family 1—Template 70049378, (b) Family 2—Template 70060673, and (c) Family 3—Template 70175408. Locations of the selected families are shown by the asterisks in Figure 2.

Cv $>$ 1 signifies temporal clustering such as during mainshock-aftershock sequences (Kagan & Jackson, 1991; Schoenball & Ellsworth, 2017a).

Figure 4 shows the cumulative event curves for all 130 prolific families colored according to Cv; the cumulative event curves are normalized such that the event count is divided by the total number of events in each family and the time is divided by the total duration of each family. As was shown for three families in Figure 3, we observe that the families reflect a wide range of behavior with Cv ranging from 1 (Poissonian) to over 7 (highly clustered). We also note that for moderately to strongly clustered families (Cv $>$ 4), the majority of events ($>$80%) tend to occur in the first half of the sequence duration. Only a few of the families with Cv $>$4 exhibit low levels of seismicity over an extended period prior to the occurrence of the main cluster of the events.

3.3. Characteristics of Prolific Families

We compare the characteristics of the Poissonian-distributed families to the more clustered sequences. The effective duration of the sequence (difference between the 10th and 90th percentiles of the origin times) is strongly anticorrelated with Cv (Figure 5a). The regularly occurring sequences have much longer effective

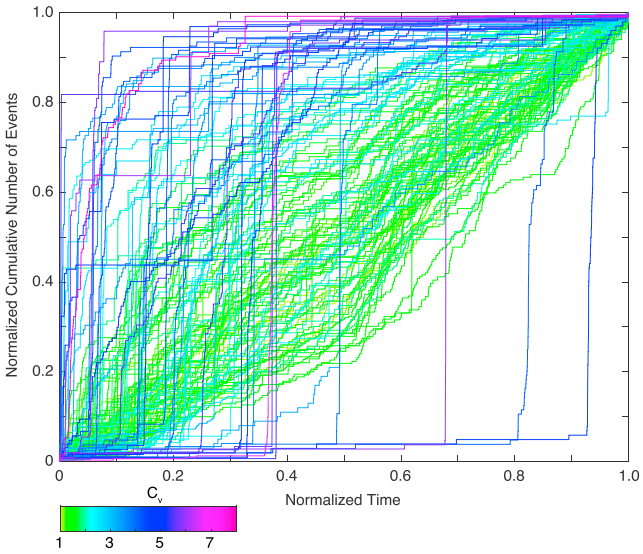

Figure 4. Normalized cumulative event curves. Cumulative event curves for each of the prolific families. The curves are normalized by number of events in each family and the total duration of each sequence. The curves are colored by the coefficient of variation (Cv) of the interevent times (see text for details) with yellow to green colors indicating families with near-Poissonian distributions and blue to purple colors indicating more clustered families.

durations with many active throughout nearly the entirety of the study period (>1,000 days), while the more clustered families have short effective durations (<200 days). The trends between Cv and duration are not just a function of spreading events out over a longer period; the sequences with higher Cv include comparatively more short absolute interevent times as shown for three families in Figure 3. And, we find that the effective start (10th percentile of the origin times) of the families with Cv near one all occur early in the study period, while families with higher Cv tend to start later (Figure 5b). And, we find an inverse correlation between Cv and the effective end (90th percentile of the origin times) of the sequences (Figure 5c), and most of the families with low Cv remain active through the end of the study period. Note that the effective start times have values beginning about 200 days after 21 March 2014, due to the initially sparse local network. We find little to no correlation between Cv template depth or number of detections (Figures 6a and 6b). We find a weak correlation between Cv and maximum magnitude (Figure 6c). Similarly, we find a weak trend between Cv and the median magnitude of a family, such that Poissonian-distributed families have lower average median magnitudes (M ~−0.19 for families with Cv < 2) than for more clustered families (M ~0.17 for families with Cv > 4). Note that the correlation between median magnitude and Cv may be due to a spatially variable magnitude of completeness.

We find that there is a distinct spatial distribution of Cv values in the study area (Figure 7a). Clusters of prolific families in the west-northwest of the study area located adjacent to high volume wastewater injection and where pressure perturbations are expected to be larger (see supporting information and Figure S3) have more regular interevent times (low Cv values). The highest Cv values are observed for the families across the remainder of the study region, generally at larger distances to injection. Additionally, the families with Cv ~1 are concentrated in areas of complex faulting that show both normal and strike-slip mechanisms (Rubinstein et al., 2018; Schoenball & Ellsworth, 2017b), while some of the highest values of Cv are for prolific families located along the structure associated with the M4.9 Milan earthquake (Figures 7b–7d).

4. Discussion

Using a matched filter technique we are able to increase by a factor of 20 the number of detected earthquakes in a region of induced seismicity in southern Kansas. We detect 130 prolific families of 100 or more events with nearly identical phase arrival differences and very similar waveform characteristics. We conclude that detections associated with a single template represent either slip on a single section of a shear fracture or adjacent shear fractures. Families of co-located earthquakes have been observed to occur not only primarily along creeping faults (Beeler et al., 2001; Nadeau & McEvilly, 1999; Vidale et al., 1994) but also in regions of high heat flow (Ross, Rollins, et al., 2017; Shelly et al., 2016). A limited number of studies have observed families of induced earthquakes associated with fluid injection (Baisch & Harjes, 2003; Lengliné et al., 2014; Zoback & Harjes, 1997). Interevent times of event families have been used to infer the rate of fault slip (Nadeau & McEvilly, 1999) and changes in fault properties (Vidale et al., 1994).

We quantify the time evolution of the prolific families and find Cv values between 1 and ~7 across the study region. Schoenball and Ellsworth (2017a) reported a similar range of Cv values in a broad scale study of earthquake behavior in Oklahoma and Kansas. Here we observe that the distribution of the coefficient of variation of interevent times depends qualitatively on the proximity of prolific families to regions of larger pressure perturbations, for example, near high-volume disposal wells. Families located closest to high rate disposal wells have interevent time distributions that are essentially Poissonian (Cv ~1; Kagan & Jackson, 1991); all families with Cv < 2 are located within 10 km of the high volume disposal wells. In the Poisson model of earthquake occurrence, constant stressing rate conditions are reflected in steady earthquake rates (Dieterich, 1994). Thus, close to disposal wells, earthquake occurrence in the prolific families appears to be

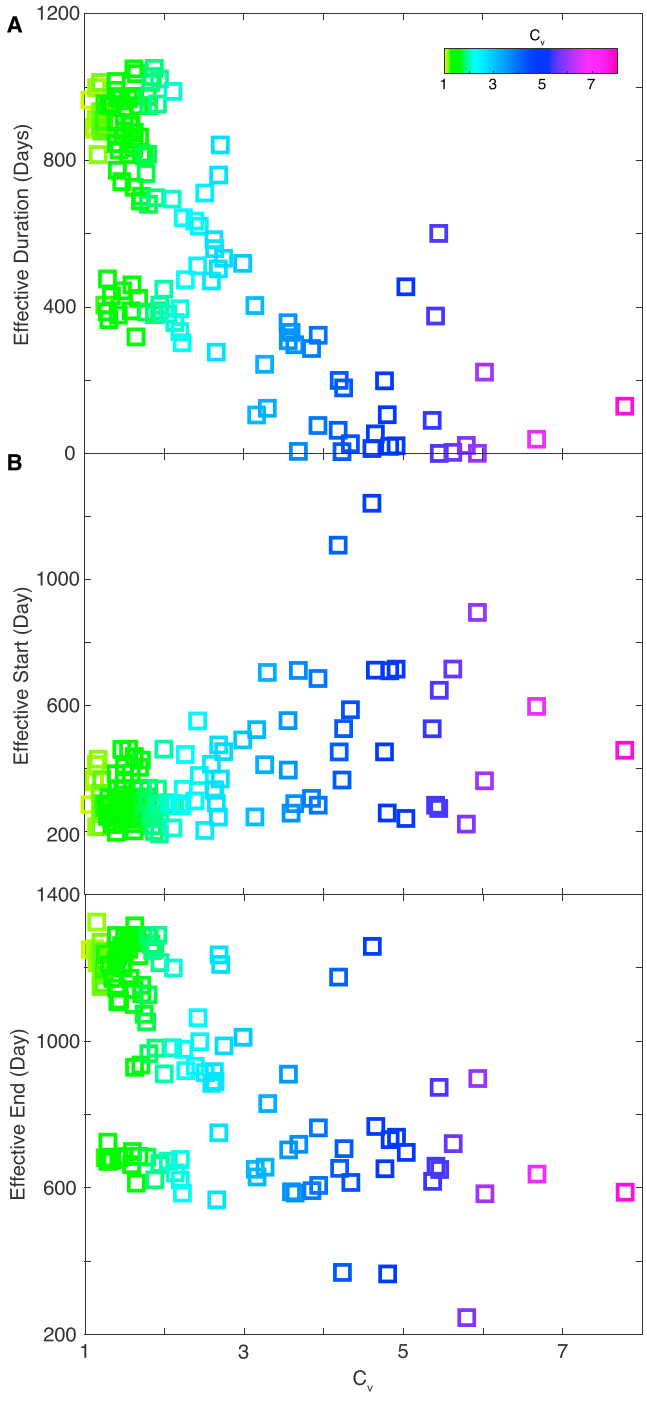

Figure 5. Time characteristics of prolific families. Coefficient of variation (Cv) of the interevent times versus (a) effective duration (difference between the 90th and 10th percentiles of the origin times) in days for each family, (b) effective start time (10th percentile of the origin time) in days after 21 March 2014 of each family, and (c) effective end time (90th percentile of the origin time) in days after 21 March 2014 of each family.

controlled by a constant driving stress. Event rates in this region of southern Kansas are well above background seismicity rates (Peterie et al., 2018; Rubinstein et al., 2018), precluding tectonic loading as the driving stress. Instead, these earthquakes are likely driven by local injection and we will explore possible mechanisms in greater detail below.

Families at greater distances from wells have higher Cv values suggesting events in these families are temporally clustered (Kagan & Jackson, 1991). Temporal clustering is observed in mainshock-aftershock sequences or swarms and reflects a non-stationary process such as a step-change in the stress due to a large nearby earthquake (Dieterich, 1994). We infer that the interevent time distributions in families with Cv $>$ 2 are primarily controlled by earthquake-earthquake interactions. So while the initial event(s) in a region may be induced either via pore-pressure changes or poroelastic stresses due to injection, subsequent events are occurring in response to a local, temporary step-change in stress. We also qualitatively observe that families with some of the highest Cv values are located along the structure involved in the Milan sequence, while lower Cv families appear in areas of mixed faulting styles (Figures 7b–7d). It is possible that in a given region the size, material properties (e.g., effective friction) and/or orientations (strike-slip versus normal) of preexisting shear fractures plays a role in controlling the interevent time distributions, but the specific mechanism for such a relationship is not clear.

We observe few prolific families within 3–5 km of the high volume disposal wells located in the southwest portion of the study area. Similarly, Rubinstein et al. (2018) also noted the relative lack of earthquakes in this region. In previous studies of other induced sequences, it has been observed that induced earthquakes occur close to disposal wells early in the sequence and then migrate outward, resulting in a donut hole in the seismicity at the location of the well (Baisch & Harjes, 2003). This phenomenon, often termed the Kaiser effect, is observed once stress begins to decrease, after the maximum stress is reached in an area (Lavrov, 2003). However, here the lack of seismicity near the wells is consistent across the entire period of injection and is not a function of the spatial or temporal availability of the seismic data (Rubinstein et al., 2018). Therefore, another mechanism is required to explain this lack of events close to wells, such as lack of available fractures or faults, as preferred by Rubinstein et al. (2018). We also examine whether the end date of prolific families correlates with the distance to the wells in order to test whether sequences close to wells end earlier than that those at greater distances. However, we observe that sequences close to wells are active throughout the entire study period (Figure 5), so additional future observations are needed to identify the end of the sequences.

Next, we consider mechanisms to explain the Poisson-distributed interevent times for families located close to disposal wells. One interpretation of these events is that they represent regular failure of essentially co-located fault patches. Repeating earthquakes in tectonic environments are most commonly interpreted as rate weakening (seismic) asperities embedded in a fault that is broadly rate strengthening (aseismic; Nadeau & McEvilly, 1999; Vidale et al., 1994). Thus, the rate of the aseismic creep on the fault surrounding the asperity controls the time between slip events (Beeler et al., 2001). Interevent times may reflect the portion of the fault that is rate strengthening based on observations that the median size and recurrence times of repeated low frequency earthquakes decrease with increasing depth in the transition zone from velocity weakening behavior to velocity strengthening (Shelly & Johnson, 2011). This

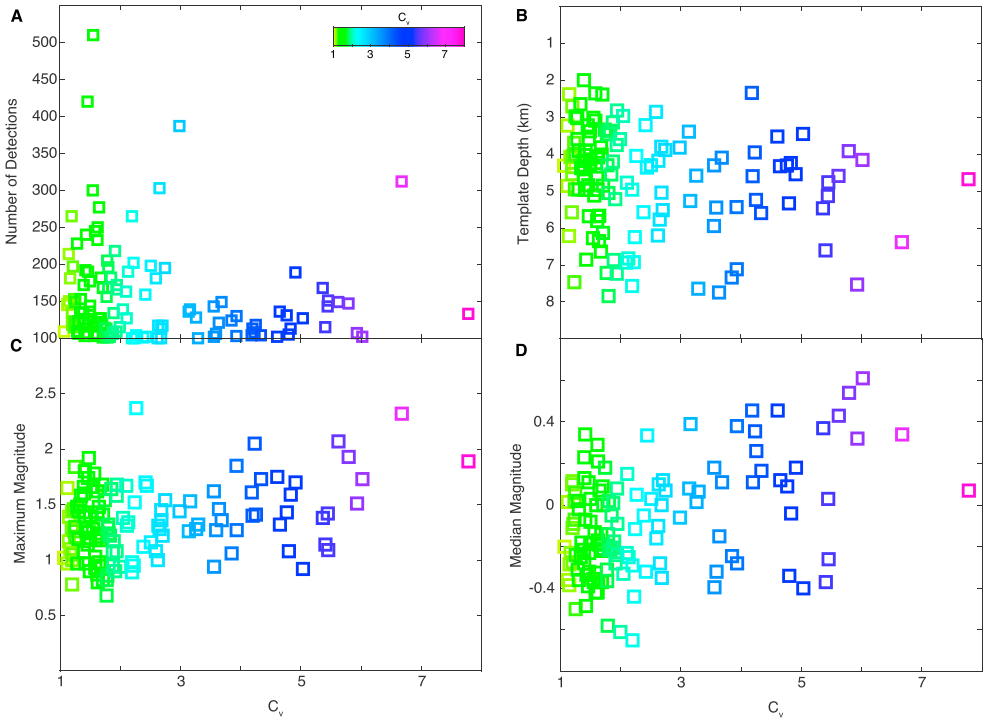

Figure 6. Additional characteristics of prolific families. Coefficient of variation (Cv) of the interevent times versus (a) number of detections, (b) template depth, (c) maximum magnitude in the family, and (d) median magnitude in the family.

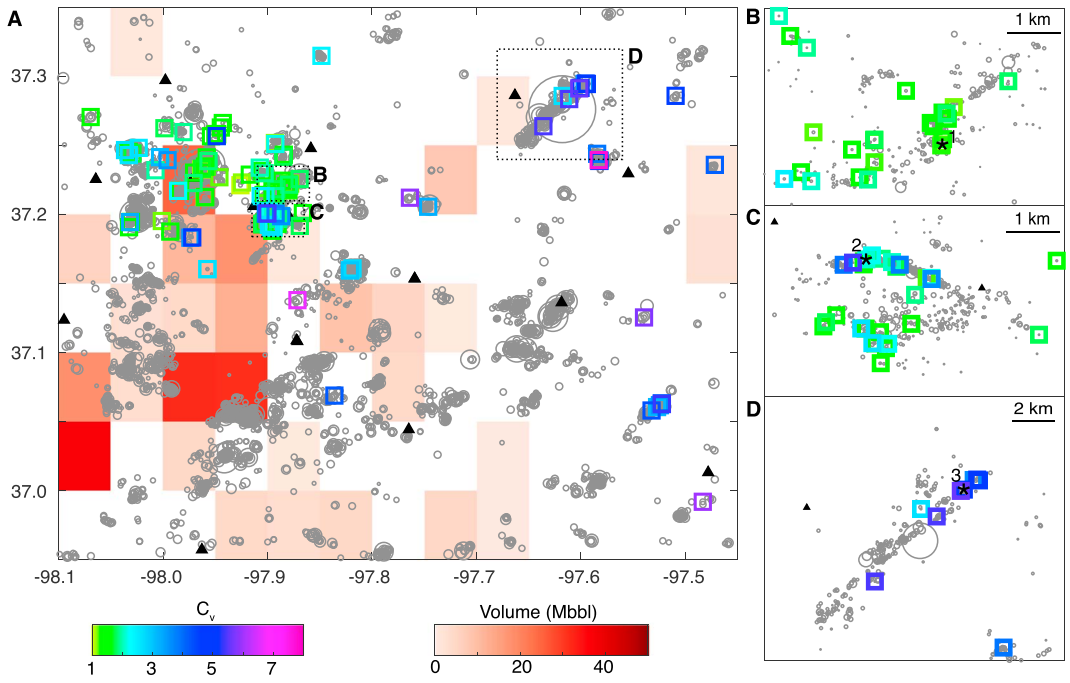

Figure 7. Spatial distribution of C_v. Map showing prolific families (squares) colored by the coefficient of variation (Cv) of the interevent times for (a) the study area with details shown for (b–d) three subareas. Well volumes are shown by the red surface as in Figure 2. Template event locations are shown by gray circles and scaled by magnitude as in Figure 1. Station locations are shown as triangles. The asterisks in (b)–(d) are the three events as shown in Figure 3.

behavior may occur near injection sites if pore fluid pressures are increased to near lithostatic, causing the effective normal stresses to go to zero such that slip behavior will transition from seismic to aseismic (Guglielmi et al., 2015; Lengliné et al., 2014). Direct measurements of fault slip and seismicity induced by injection into a natural fault at the Coaraze laboratory site in France show slip were predominantly accommodated aseismically, with microearthquakes mediated by aseismic creep (Guglielmi et al., 2015). The diffuse nature of the seismicity observed close to wells would require a large number of sizeable aseismically slipping structures; without additional data it is difficult to confirm whether or not aseismic slip is occurring.

Baisch and Harjes (2003) propose an alternate model to explain clusters of seismicity with similar waveforms observed during the KTB, Germany injection. In this model, fluid pressures within the facture network are controlled by a spatially variable permeability. Slip occurs when critical pore fluid pressure is reached and the Coulomb-failure criterion is met, such that the ratio of shear to normal effective stress becomes larger than the coefficient of friction. Baisch and Harjes (2003) assume that the fracture system includes a range of fracture orientations such that well-oriented fractures fail repeatedly, while surrounding fractures do not fail. Multiple failure of the same fracture occurs only if fluid pressures continue to increase. Interevent times are constant if fluid pressures linearly increase and stress drops are similar between successive events in a family.

If we assume the model of Baisch and Harjes (2003), then for prolific families to occur throughout the study period, nearby fluid pressures to increase with time for repeated slip are required. Peterie et al. (2018) show bottomhole pressures in the Arbuckle increase from 2014 through the end of 2016 from readings at several Class I wells located at distances ranging from approximately 40 to 150 km from high volume injection. Pressure evolution within the basement is likely more complex than within the injection reservoir as fluid pathways are dependent on the availability of permeable fractures (e.g., Hsieh & Bredehoeft, 1981), but the pressure evolution likely follows a similar trend of increasing pressures through time as observed in the Arbuckle.

Following Baisch and Harjes (2003), rate of pore pressure change can be assumed to be proportional to the earthquake stress drop divided by the earthquake interevent times. Explicitly, we assume the rate pressure increase is equal to the stress drop estimated using the median magnitude of a family multiplied by the number of events in a sequence and divided by the coefficient of friction. Due to the small magnitudes of the events we are unable to estimate reliable stress drops, so we estimate the expected stress drops from previous studies. Studies suggest that small to moderate size induced earthquakes in Oklahoma and Kansas have low stress drops and are not self-similar (Sumy et al., 2017; Trugman et al., 2017).

We estimate the upper bound of pressure increase for Family 1 (Template 70049378) that has a mean interevent time of 10.3 days (Figure 3a). Using the scaling relationship between moment and stress drop for the Kansas template catalog provided by Trugman et al. (2017), we estimate a stress drop for each event in Family 1. Summing the stress drops of the events and assuming a coefficient of friction of 0.6, we find as an upper bound of pressure increase 2.6 MPa/year over the 3.3 years the family is active. This value represents an upper bound on the pressure increase due to our assumption that repeated failure occurs on a single patch of fault. Repeating the analysis for all families with $Cv < 2$, we find a median upper bound of pressure increase of 4.3 MPa/year with a range of values between 2.1 and 15.9 MPa/year. The pressure changes we estimate are larger than pressure changes that we estimate for the Arbuckle (Figure S3) and significantly larger than those previously estimated through pore pressure modeling of injection in Oklahoma (Barbour et al., 2017; Goebel et al., 2017; Keranen et al., 2014). And, at a Class I well (HP2) located north of the study region the total observed pressure increase in the Arbuckle is 0.5 MPa over a 4-year period, with a maximum of 0.14 MPa/year, as reported by Peterie et al. (2018).The unexpectedly high median upper bound of pressure increase may suggest that slip within a family occurs on closely spaced subparallel or adjacent fault patches rather than repeated slip on the same patch; alternately, timing of failure may be controlled by a different mechanism that is as of yet unknown.

5. Conclusions

We conclude that families of near-repeating events that are located close to high-rate injection wells show distinctive interevent time behavior when compared to sequences where pressure changes are lower. Interevent times of families within 5 to 10 km of high-rate wells are near-Poissonian, which may suggest

that the sequences are being directly driven by increases in pore fluid pressure. And, while local wastewater disposal induces seismicity across the region, families farther from high-rate wells show a high degree of clustering that may indicate that timing of events in those sequences is dominated by earthquake-earthquake interactions along well-defined shear fractures.

Acknowledgments
Waveform data from the GS and OK seismic networks used in the analysis are available from Incorporated Research Institutions for Seismology (IRIS) data archive. We thank N. Beeler and N. van der Elst and two anonymous journal reviewers for helpful comments that improved the manuscript.

References

Baisch, S., & Harjes, H.-P. (2003). A model for fluid-injection-induced seismicity at the KTB, Germany. *Geophysical Journal International*, *152*(1), 160–170. https://doi.org/10.1046/j.1365-246X.2003.01837.x

Barbour, A. J., Norbeck, J. H., & Rubinstein, J. L. (2017). The effects of varying injection rates in Osage County, Oklahoma, on the 2016 Mw 5.8 Pawnee earthquake. *Seismological Research Letters*, *88*, 1040–1053. https://doi.org/10.1785/0220170003

Beeler, N. M., Lockner, D. L., & Hickman, S. H. (2001). A simple stick-slip and creep-slip model for repeating earthquakes and its implication for microearthquakes at Parkfield. *Bulletin of the Seismological Society of America*, *91*(6), 1797–1804.

Blanpied, M. L., Lockner, D. A., & Byerlee, J. D. (1992). An earthquake mechanism based on rapid sealing of faults. *Nature*, *358*(6387), 574–576. https://doi.org/10.1038/358574a0

Bufe, C. G., Harsh, P. W., & Buford, R. O. (1977). Steady-state seismic slip—Precise recurrence model. *Geophysical Research Letters*, *4*(2), 91–94. https://doi.org/10.1029/GL004i002p00091

Byerlee, J. (1993). Model for episodic flow of high-pressure water in fault zones before earthquakes. *Geology*, *21*(4), 303–306. https://doi.org/10.1130/0091-7613(1993)021<0303:MFEFOH>2.3.CO;2

Cornet, F. H., Helm, J., Poitrenaud, H., & Etchecopar, A. (1997). Seismic and aseismic slips induced by larger-scale fluid injections. *Pure and Applied Geophysics*, *150*(3-4), 563–583. https://doi.org/10.1007/s000240050093

Dieterich, J. (1994). A constitutive law for rate of earthquake production and its application to earthquake clustering. *Journal of Geophysical Research*, *99*(B2), 2601–2618. https://doi.org/10.1029/93JB02581

Ellsworth, W. (2013). Injection-induced earthquakes. *Science*, *341*(6142), 1225942–149. https://doi.org/10.1126/science.1225942

Franseen, E. K., Byrnes, A. P., Cansler, J. R., & Carr, T. (2004). The geology of Kansas–Arbuckle Group. Lawrence, KS: Kansas Geological Survey.

Gardner, J. K., & Knopoff, L. (1974). Is the sequence of earthquakes in southern California, with aftershocks removed, Poissonian. *Bulletin of the Seismological Society of America*, *64*, 1363–1367.

Geller, R. J., & Mueller, C. S. (1980). Four similar earthquakes in central California. *Geophysical Research Letters*, *7*(10), 821–824. https://doi.org/10.1029/GL007i010p00821

Goebel, T. H. W., Weingarten, M., Chen, X., Haffener, J., & Brodsky, E. E. (2017). The 2016 Mw5.1 Fairview, Oklahoma earthquakes: Evidence for long-range poroelastic triggering at >40 km from fluid disposal wells. *Earth and Planetary Science Letters*, *472*, 50–61. https://doi.org/10.1016/j.epsl.2017.05.011

Guglielmi, Y., Cappa, F., Avouac, J.-P., Henry, P., & Elsworth, D. (2015). Seismicity triggered by fluid injection-induced aseismic slip. *Science*, *348*(6240), 1224–1226. https://doi.org/10.1126/science.aab0476

Healy, J. H., Rubey, W. W., Griggs, D. T., & Raleigh, C. B. (1968). The Denver earthquakes. *Science*, *161*(3848), 1301–1310. https://doi.org/10.1126/science.161.3848.1301

Horton, S. (2012). Disposal of hydrofracking waste fluid by injection into subsurface aquifers triggers earthquake swarm in central Arkansas with potential for damaging earthquake. *Seismological Research Letters*, *83*(2), 250–260. https://doi.org/10.1785/gssrl.83.2.250

Hsieh, P. A., & Bredehoeft, J. D. (1981). A reservoir analysis of the Denver earthquakes: A case of induced seismicity. *Journal of Geophysical Research*, *86*(B2), 903–920. https://doi.org/10.1029/JB086iB02p00903

Kagan, Y. Y., & Jackson, D. D. (1991). Long-term earthquake clustering. *Geophysical Journal International*, *104*(1), 117–134. https://doi.org/10.1111/j.1365-246X.1991.tb02498.x

Keranen, K. M., Savage, H. M., Abers, G. A., & Cochran, E. S. (2013). Potentially induced earthquakes in Oklahoma, USA: Links between wastewater injection and the 2011 Mw 5.7 earthquake sequence. *Geology*, *41*(6), 699–702. https://doi.org/10.1130/G34045.1

Keranen, K. M., Weingarten, M., Abers, G. A., Bekins, B. A., & Ge, S. (2014). Sharp increase in central Oklahoma seismicity since 2008 induced by massive wastewater injection. *Science*, *345*(6195), 448–451. https://doi.org/10.1126/science.1255802

Kroll, K. A., Richards-Dinger, K. B., & Dieterich, J. H. (2017). Sensitivity of induced seismic sequences to rate-and-state frictional processes. *Journal of Geophysical Research: Solid Earth*, *122*, 10,207–10,219. https://doi.org/10.1002/2017JB014841

Lavrov, A. (2003). The Kaiser effect in rocks: Principles and stress estimation techniques. *International Journal of Rock Mechanics and Mining Sciences*, *40*(2), 151–171. https://doi.org/10.1016/S1365-1609(02)00138-7

Lengliné, O., Lamourette, L., Vivin, L., Cuenot, N., & Schmittbuhl, J. (2014). Fluid-induced earthquakes with variable stress drop. *Journal of Geophysical Research: Solid Earth*, *119*, 8900–8913. https://doi.org/10.1002/2014JB011282

Morgan, B. C., & Murray, K. E. (2015). *Characterizing small-scale permeability of the Arbuckle Group*, Oklahoma. Oklahoma Geological Survey Open-File Report OFR2–OFR2015. Norman, OK: Oklahoma Geological Survey.

Nadeau, R. M., & Johnson, L. R. (1998). Seismological studies at Parkfield VI: Moment release rates and estimates of source parameters for small repeating earthquakes. *Bulletin of the Seismological Society of America*, *88*, 790–814.

Nadeau, R. M., & McEvilly, T. V. (1999). Fault slip rates at depth from recurrence intervals of repeating microearthquakes. *Science*, *285*(5428), 718–721. https://doi.org/10.1126/science.285.5428.718

Nicholson, C., & Wesson, R. L. (1990). Earthquake hazard associated with deep well injection. *U.S. Geological Survey Bulletin*, *1951*. 74 pp., doi: https://doi.org/10.3133/b1951

Niemi, T. M. (2004). Investigation of microearthquakes, macroseismic data, and liquefaction associated with the 1867 Wamego earthquake in eastern Kansas. *Bulletin of the Seismological Society of America*, *94*(6), 2317–2329. https://doi.org/10.1785/0120030101

Parotidis, M., Shapiro, S. A., & Rothert, E. (2005). Evidence for triggering of the Vogtland swarms 2000 by pore pressure diffusion. *Journal of Geophysical Research*, *110*, B05S10. https://doi.org/10.1029/2004JB003267

Peterie, S. L., Miller, R. D., Intfen, J. W., & Gonzales, J. B. (2018). Earthquakes in Kansas induced by extremely far-field pressure diffusion. *Geophysical Research Letters*, *45*, 1395–1401. https://doi.org/10.1002/2017GL076334

Petersen, M. D., Mueller, C. S., Moschetti, M. P., Hoover, S. M., Rubinstein, J. L., Llenos, A. L., et al. (2015). *Incorporating induced seismicity in the 2014 United States seismic hazard model—Results of the 2014 workshop and sensitivity studies*, U.S. Geological Survey Open-File Report 2015–1070 69 p. https://doi.org/10.3133/ofr20151070

Raleigh, C. B., Healy, J. H., & Bredehoeft, J. D. (1976). An experiment in earthquake control at Rangely, Colorado. *Science*, *191*(4233), 1230–1237. https://doi.org/10.1126/science.191.4233.1230

Ross, Z. E., Hauksson, E., & Ben-Zion, Y. (2017). Abundant off-fault seismicity and orthogonal structures in the San Jacinto fault zone. *Science Advances*, *3*(3), e1601946. https://doi.org/10.1126/sciadv.1601946

Ross, Z. E., Rollins, C., Cochran, E. S., Hauksson, E., Avouac, J.-P., & Ben-Zion, Y. (2017). Aftershocks driven by afterslip and fluid pressure sweeping through a fault-fracture mesh. *Geophysical Research Letters*, *44*, 8260–8267. https://doi.org/10.1002/2017GL074634

Rubinstein, J. L., Ellsworth, W. L., & Dougherty, S. L. (2018). The 2013-2016 induced earthquakes in Harper and Sumner counties, southern Kansas. *Bulletin of the Seismological Society of America*, *108*(2), 674–689. https://doi.org/10.1785/0120170209

Schoenball, M., & Ellsworth, W. L. (2017a). A systematic assessment of the spatiotemporal evolution of fault activation through induced seismicity in Oklahoma and southern Kansas. *Journal of Geophysical Research: Solid Earth*, *122*, 10,189–10,206. https://doi.org/10.1002/2017JB014850

Schoenball, M., & Ellsworth, W. L. (2017b). Waveform relocated earthquake catalog for Oklahoma and southern Kansas illuminates the regional fault network. *Seismological Research Letters*, *88*(5), 1252–1258. https://doi.org/10.1785/0220170083

Schwab, D., Bigdoli, T., & Taylor, M. H. (2017). Characterizing the potential for injection-induced fault reactivation through subsurface structural mapping and stress field analysis, Wellington field, Sumner County, Kansas. *Journal of Geophysical Research: Solid Earth*, *122*, 10,132–10,154. https://doi.org/10.1002/2017JB014071

Shelly, D. R., Ellsworth, W. L., & Hill, D. P. (2016). Fluid-faulting evolution in high definition: Connecting fault structure and frequency-magnitude variations during the 2014 Long Valley Caldera, California, earthquake swarm. *Journal of Geophysical Research: Solid Earth*, *121*, 1776–1795. https://doi.org/10.1002/2015JB012719

Shelly, D. R., & Johnson, K. M. (2011). Tremor reveals stress shadowing, deep postseismic creep, and depth-dependent slip recurrence on the lower-crustal San Andreas fault near Parkfield. *Geophysical Research Letters*, *38*, L13312. https://doi.org/10.1029/2011GL047863

Sibson, R. H. (1992). Implications of fault-valve behavior for rupture nucleation and recurrence. *Tectonophysics*, *211*(1-4), 283–293. https://doi.org/10.1016/0040-1951(92)90065-E

Sumy, D. F., Neighbors, C. J., Cochran, E. S., & Keranen, K. M. (2017). Low stress drops observed for aftershocks of the 2011 Mw 5.7 Prague, Oklahoma, earthquake. *Journal of Geophysical Research: Solid Earth*, *122*, 3813–3834. https://doi.org/10.1002/2016JB013153

Talwani, P., Chen, L., & Gahalaut, K. (2007). Seismogenic permeability, k_s. *Journal of Geophysical Research*, *112*, B07309. https://doi.org/10.1029/2006JB004665

Trugman, D. T., Dougherty, S. L., Cochran, E. S., & Shearer, P. M. (2017). Source spectral properties of small to moderate earthquakes in southern Kansas. *Journal of Geophysical Research: Solid Earth*, *122*, 8021–8034. https://doi.org/10.1002/2017JB014649

Vidale, J. E., Ellsworth, W. L., Cole, A., & Marone, C. (1994). Variations in rupture process with recurrence interval in a repeated small earthquake. *Nature*, *368*(6472), 624–626. https://doi.org/10.1038/368624a0

Walsh, F. R., & Zoback, M. D. (2015). Oklahoma's recent earthquakes and saltwater disposal. *Science Advances*, *1*(5), e1500195. https://doi.org/10.1126/sciadv.1500195

Wang, H. F. (2000). *Theory of linear poroelasticity*. Princeton, NJ: Princeton University Press.

Wei, S., Avouac, J.-P., Hudnut, K. W., Donnellan, A., Parker, J. W., Graves, R. W., et al. (2015). The 2012 Brawley swarm triggered by injection-induced aseismic slip. *Earth and Planetary Science Letters*, *422*, 115–125. https://doi.org/10.1016/j.epsl.2015.03.054

Zoback, M. D. (2007). *Reservoir geomechanics*. Cambridge, UK: Cambridge University Press. https://doi.org/10.1017/CBO9780511586477

Zoback, M. D., & Harjes, H.-P. (1997). Injection-induced earthquakes and crustal stress at 9 km depth at the KTB deep drilling site, Germany. *Journal of Geophysical Research*, *102*(B8), 18,477–18,491. https://doi.org/10.1029/96JB02814